Mesoporous Materials

DOI: 10.1002/ange.201202232

Synthesis of Dual-Mesoporous Silica Using Non-Ionic Diblock Copolymer and Cationic Surfactant as Co-Templates**

Jing Wei, Qin Yue, Zhenkun Sun, Yonghui Deng, and Dongyuan Zhao**

Ordered mesoporous materials, ever since their discovery,[1] have attracted considerable interest owing to their outstanding physicochemical properties (such as high surface area, large pore volume, variety of pore structures, easily modifiable surface, diverse framework compositions) and broad potential applications in, for example, adsorption,[2] separation,[3] catalysis,[4] drug delivery[5] and fuel cells.[6] Considerable efforts have recently been devoted to fabricating ordered porous materials with hierarchical pore structures, such as macro-/meso-,[7] meso-/micro-,[8] and macro-/microporous materials.[9] Additionally, in order to further increase the surface area for enhanced interactions with adsorbents and reduced transport limitations, much research has been conducted on the synthesis of ordered mesoporous materials with a bimodal pore structure which are highly desirable for applications in catalysis, sensing, and drug delivery.[10–13]

According to the templating synthesis concept for mesoporous materials, the bimodal mesopore system can be achieved by using two templates of different molecular weights that lead to pores of corresponding pore sizes. In fact, various template pairs have been employed to synthesize mesoporous materials with bimodal pores, including a non-ionic copolymer and an ionic surfactant,[10] a non-ionic copolymer and a non-ionic surfactant,[11] an ionic block copolymer and an ionic surfactant,[12] and mixed templates of two block copolymers with different molecular weights.[13] However, in most cases dual-mesoporous materials with well-defined pore arrangements (specifically, with small mesopores surrounding the large mesopores) and tunable pore sizes could not be synthesized because of difficulties in controlling the assembly process in the dual-templating system. From a general thermodynamic point of view, the creation of a hierarchical micellar system is usually unfavorable; the two template molecules tend to form either mixed micelles or they form separate macroscopic phases.[14] In light of this theoretical consideration, to achieve a hierarchical mesostructure, it is necessary for one set of template molecules to form stable micelles first before interaction with the second set of template molecules during the synthesis process. Consequently, to obtain ordered dual-mesoporous materials with two well-arranged sets of mesopores, two obstacles must be overcome. One is forming distinct large micelles of high-molecular-weight block copolymers and small micelles of low-molecular-weight surfactants. The second obstacle is triggering the independent co-assembly of the two kinds of micelles into an organized "alloy" phase, with small surfactant molecules filling the interstitial voids of the ordered mesostructure built up by large block copolymers. However, to date, it is a challenge to control the assembly process in the synthesis of dual-mesoporous silica with two kinds of template molecules.

We report herein on a solvent-evaporation-induced step-by-step aggregating approach for the synthesis of ordered dual-mesoporous silica materials by using poly(ethylene oxide)-*block*-poly(methyl methacrylate) (PEO-*b*-PMMA) and alkyltrimethylammonium bromide (C_nTAB) as co-templates and tetraethyl orthosilicate (TEOS) as a silica source in an acidic tetrahydrofuran (THF)/H_2O solution. It is found that, at the early stage of THF solvent evaporation, PEO-*b*-PMMA copolymers with associated silicate oligomers first formed stable composite micelles in the solution. With the further evaporation of THF, the increased concentration and strong electrostatic attraction induce C_nTAB molecules to move toward the negatively charged spherical composite micelles. Further evaporation of THF causes the composite micelles to assemble into large particles (0.5–6.0 μm) with a face-centered-cubic (*fcc*) structured mesophase. Meanwhile, the ultrahigh concentration of C_nTAB molecules located in the interstitial space of the aggregated composite micelles assemble into curving rod-shaped micelles, resulting in a unique ordered mesostructure constructed of spherical large micelles and wormlike small micelles bound with silicate species (Scheme 1). After the templates were removed by simple calcination in air, unique ordered dual-mesoporous silica materials were obtained with large mesopores (ca. 20 nm) packed in an $Fm\bar{3}m$ structure and small wormlike mesopores (ca. 2.5 nm) homogeneously distributed in the wall of the large pores.

Because the non-ionic EO_{125}-MMA_{174} has a very long hydrophobic segment, a mixture of THF and aqueous hydrochloric acid solution (3:1 v/v) was used to dissolve this template, the ionic surfactants, and the silica source (TEOS), yielding a homogeneous starting solution. It was found that, similar to our previous report,[15] as the THF evaporated, the reaction system underwent a dramatic change from a clear solution, to a blue colloidal dispersion, to a white turbid

[*] J. Wei, Q. Yue, Z. K. Sun, Prof. Dr. Y. H. Deng, Prof. Dr. D. Y. Zhao
Department of Chemistry and Advanced Materials Laboratory
Fudan University, Shanghai 200433 (P.R. China)
E-mail: yhdeng@fudan.edu.cn
dyzhao@fudan.edu.cn
Homepage: http://www.mesogroup.fudan.edu.cn/

[**] This work was supported by the NSF of China (20890123, 20821140537, and 21073040), the State Key 973 Program of PRC (2012CB224805), Shanghai Leading Academic Discipline Project (B108), the Science & Technology Commission of Shanghai Municipality (08DZ2270500), and the Key Subjects Innovative Talents Training Program of Fudan University.

Supporting information for this article is available on the WWW under http://dx.doi.org/10.1002/anie.201202232.

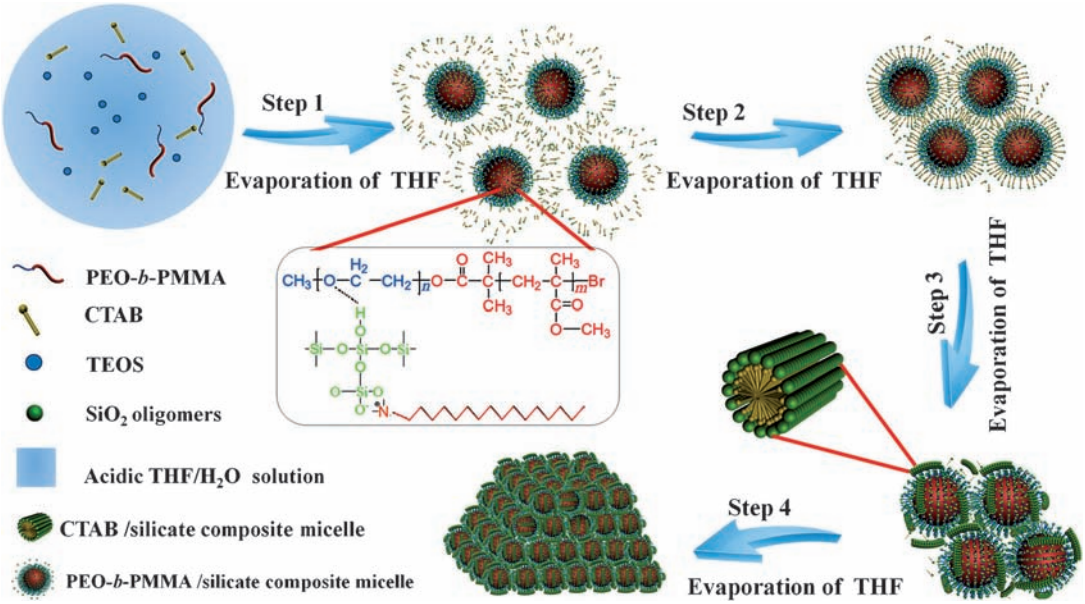

Scheme 1. The formation process of ordered dual-mesoporous silica materials.

suspension, and finally to a residual suspension with a white precipitate deposited at the bottom of the vial. The small-angle X-ray scattering (SAXS) pattern of the collected sample, the as-made ordered dual-mesoporous silica prepared with C_{16}TAB as the small template at 25 °C (denoted as ODMS-C_{16}-25), exhibits four peaks in the q range of 0.2–0.8 nm^{-1}, which can be indexed to the 111, 220, 531, and 731 reflections of highly ordered *fcc* mesostructure with a space group of $Fm\bar{3}m$ (see Figure S1 in the Supporting Information). The broad peak at a q value of approximately 1.5 nm^{-1} indicates the coexistence of the smaller-scale mesostructure constructed by the C_{16}TAB templates. After the two sets of templates had been removed by calcination at 550 °C in air, the SAXS pattern of the ordered dual-mesoporous silica (denoted as ODMS-C_{16}-550) exhibits six well-resolved peaks at q values of 0.242, 0.398, 0.457, 0.612, 0.825, and 1.068 nm^{-1}, which can be indexed to the 111, 220, 311, 331, 531, and 731 reflections of an *fcc* mesostructure. The calculated unit cell parameter of ODMS-C_{16}-550 is about 44.9 nm. The shrinkage of the framework is about 14 %. The disappearance of the broad peak at a q value of 1.5 nm^{-1} after calcination is due to the structure shrinkage that degrades the ordering of the small-pore mesostructure.

Scanning electron microscope (SEM) observations indicate that ODMS-C_{16}-25 consists of irregular particles with dimensions of 0.5–6.0 μm (Figure S2a). The field-emission scanning electron microscope (FESEM) images reveal that each particle is constructed from numerous uniform nanospheres (Figure S2b). A typical hexagonal pattern of nanospheres aligned in a layer-by-layer fashion can be observed over a large domain on the surface of the particles. These results further confirm that a cubic closely packing structure (i.e. *fcc*) of the mesostructured particles is formed during the solvent-evaporation-induced aggregating assembly process, which is similar to that in a previous report.[15] After the template had been removed by calcination in air, an ordered mesoporous structure is clearly visible in the FESEM images of the ODMS-C_{16}-550 sample (Figure S2c). To observe the inner structure from the SEM images, the sample was gently ground. From the cross-section image of the particles, highly ordered arrays of mesopores can be observed throughout the whole particle (Figure S2d).

Transmission electron microscopy (TEM) was further employed to acquire more detailed information on the mesostructure. TEM images of the ODMS-C_{16}-550 taken along the 110, 100, and 211 directions (Figure 1 a–d), respectively, reveal a highly ordered mesostructure of $Fm\bar{3}m$ symmetry. The unit cell parameter estimated from TEM images (Figure 1 c) is about 45 nm, close to the value calculated from the SAXS results (Figure S1). It is worth

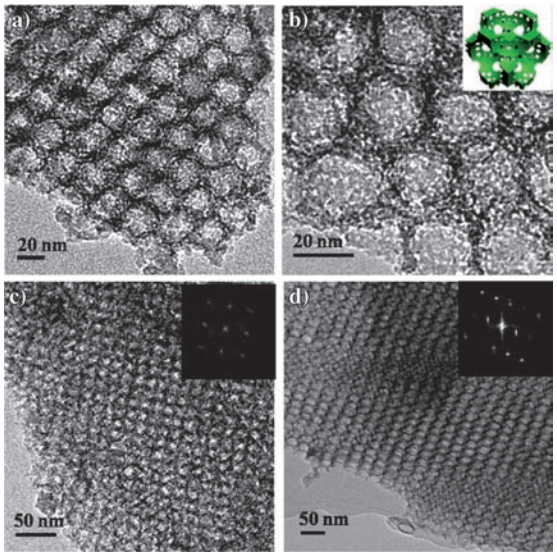

Figure 1. TEM images taken along the [110] (a, b), [100] (c), and [211] (d) directions of ODMS-C_{16}-550 prepared by using EO_{125}-MMA_{174} and C_{16}TAB as the template pair. The inset in (b) is the structural model of ODMS-C_{16}-550; the insets in (c) and (d) are the corresponding FFT diffractograms.

noting that numerous wormlike small pores of roughly 2.0 nm in diameter can be observed in the silica pore walls (Figure 1b). As a result, the silica wall is highly porous and loose, as schematically illustrated in the inset of Figure 1b. In contrast, the ordered mesoporous silica synthesized analogously but using only EO_{125}-MMA_{174} as a template has the same pore symmetry but dense pore walls, as evidenced by the SAXS and TEM characterizations (Figure S3). These results suggest that the smaller mesopores are generated by the small C_{16}TAB molecules which tend to assemble into a wormlike mesostructure around the large spherical EO_{125}-MMA_{174} micelles with the assistance of siliceous species in the solution.

Nitrogen sorption isotherms of the sample ODMS-C_{16}-550 show two capillary condensation steps in the P/P_0 ranges of 0.1–0.2 and 0.85–0.95, respectively, indicating that two sets of pores coexist in the materials (Figure 2a). The pore size distribution calculated using nonlocal density functional

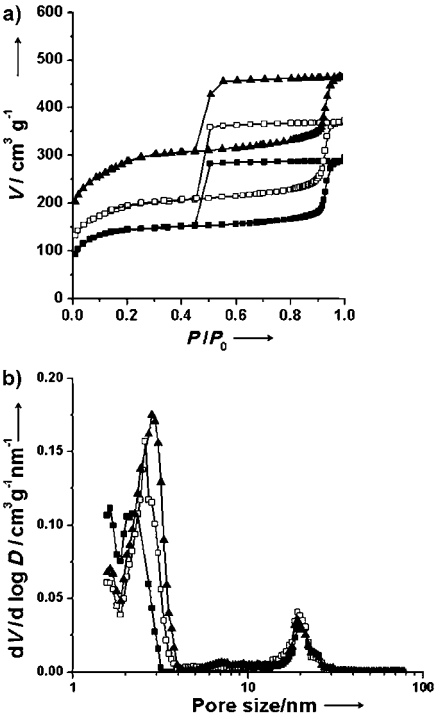

Figure 2. a) Nitrogen sorption isotherms and b) pore size distributions of ODMS-C_{14}-550 (■), ODMS-C_{16}-550 (□), and ODMS-C_{18}-550 (▲). For clarity, the isotherm curves in (a) are offset by 50 $cm^3 g^{-1}$ for ODMS-C_{16}-550 and 100 $cm^3 g^{-1}$ for ODMS-C_{18}-550, respectively.

theory (NLDFT) methods reveals two sets of pores with diameters centered at 19.2 and 2.6 nm, respectively, which can be attributed to the removal of EO_{125}-MMA_{174} and C_{16}TAB molecules, respectively (Figure 2b). The BET surface area and pore volume are calculated to be 517 $m^2 g^{-1}$ and 0.51 $cm^3 g^{-1}$ respectively.

To further study the dual-templating synthesis and tune the size of small mesopores, cationic surfactants having hydrophobic tails of different lengths, C_{14}TAB and C_{18}TAB, were also used as the co-templates in the same synthesis system as that used for the sample ODMS-C_{16}-550. SAXS patterns of the obtained ODMS-C_{14}-550 and ODMS-C_{18}-550 indicate that both samples possess the same mesostructural symmetry ($Fm\bar{3}m$) as ODMS-C_{16}-550 (Figure S4). The unit cell parameters of ODMS-C_{14}-550 and ODMS-C_{18}-550 are about 47.3 and 42.8 nm, respectively (Table S1). Similar to ODMS-C_{16}-550, the calcined samples ODMS-C_{14}-550 and ODMS-C_{18}-550 show nitrogen adsorption–desorption isotherms with two capillary condensation steps in the P/P_0 ranges of 0.1–0.2 and 0.85–0.95, respectively (Figure 2). The diameters of the small pores are calculated to be 2.2 and 2.8 nm for ODMS-C_{14}-550 and ODMS-C_{18}-550, respectively, while the diameter of the large pores of both samples remains about 20 nm. These results clearly suggest that, when cationic surfactants are used having hydrophobic tails of different lengths, the ordered mesostructure of large pores templated by the EO_{125}-MMA_{174} copolymers is retained and the size of the smaller mesopores can be readily tuneable.

Dynamic light scattering (DLS) was used to monitor the evolution of the particles formed during the synthesis process (Figure S5). For the starting solution, the particle size distribution profile shows only one peak at 4.2 nm, which is from the well-dissolved PEO-*b*-PMMA unimers (Figure S5a). After evaporation of THF for 20 h, two peaks at 0.86 and 22.3 nm can be observed, which are attributed to silicate oligomers and PEO-*b*-PMMA micelles, respectively (Figure S5b). After further evaporation for 5 h, the size of silica oligomers increases to 1.8 nm as a result of the further hydrolysis and condensation of the siliceous species. Meanwhile, the PEO-*b*-PMMA micelles increase to 37.0 nm, indicative of the association of CTAB and PEO-*b*-PMMA micelles (Figure S5c). When the solution is further concentrated after evaporation for 30 h (Figure S5d), the size of the silicate oligomers almost remains unchanged, but the composite micelles grow to sizes of 46.0 nm, implying that the PEO-*b*-PMMA micelles are surrounded by more CTAB molecules. Moreover, a new peak at about 5.5 μm is detected, indicating that the composite micelles gradually assemble into large particles by aggregation. Further prolonging the evaporation time results in a turbid suspension which is not suitable for DLS measurements.

Based on the results mentioned above, we speculate that the ordered dual-mesoporous silica materials in our dual-template synthesis form by a solvent-evaporation-induced step-by-step aggregating assembly process. In our study, because of the strong hydrophobicity of the PMMA chains, it is difficult to dissolve PEO-*b*-PMMA copolymers in water. Consequently, at the beginning, PEO-*b*-PMMA and C_nTAB molecules can be dissolved in the mixed solution containing a large amount of THF (ca. 70% by volume), a good solvent for both PEO and PMMA segments. With the evaporation of THF, the solvency power of the remaining acidic THF/H_2O solvent for the copolymers decreases significantly; simultaneously, silicate oligomers generated through the hydrolysis and condensation of TEOS can associate with the PEO segments by hydrogen bonding. As a consequence, block copolymers with associated silicate oligomers begin to assemble into spherical composite micelles with a PMMA core and a PEO/silicate shell (step 1, Scheme 1). At this stage, C_nTAB molecules, which can also associate with silicate species through electrostatic interaction, are still well dis-

solved in the solution because these short-chain cationic surfactants are soluble in both THF and water. With the further evaporation of THF, the concentration of both components (block copolymer micelles, and C_nTAB molecules and silicate species) increase significantly; at this stage (step 2, Scheme 1), C_nTAB molecules tend to approach the PEO-*b*-PMMA/silicate composite micelles because of the high density of silicate species on their surface. Meanwhile, the large composite micelles begin to aggregate and assemble into ordered mesostructure in a layer-by-layer fashion to achieve minimum interface energy. Further evaporation of THF causes the concentration of CTAB molecules in the interstitial space of the aggregated large composite micelles to increase significantly, which compels them to assemble in situ into curving short rodlike micelles (step 3, Scheme 1). The mesostructured aggregates further grow into large particles by adopting large composite micelles and CTAB molecules (step 4, Scheme 1). This multicomponent mesostructure is well fixed through the condensation of silicate species surrounding the micelles promoted by the elevated acidity of the remaining aqueous solution. Finally, the calcination in air leads to ordered dual-mesoporous silicas with large mesopores packed in an *fcc* structure and a silica wall decorated with wormlike secondary small mesopores.

The unique hierarchical mesostructure with highly interconnected pore channels, high surface area, large pore volume, and easily modifiable surface make the ordered dual-mesoporous silica an ideal candidate for various applications including catalysis, drug delivery, catalysis, adsorption ,and separation. Here, in this study, we successfully encapsulated Au nanoparticles (ca. 4.0 nm) in the mesopores of the dual-mesoporous silica using the in situ reduction method.[16] The Au/ODMS-C_{16}-550 sample obtained after the Au nanoparticles had been loaded retains the ordered mesostructure, as indicated by the TEM images (Figure 3a,b). The Au nanoparticles with a mean diameter of 4.0 nm are highly dispersed in the dual-mesoporous silica matrices. The high-magnification TEM image (Figure 3a, inset) reveals that Au nanoparticles are mainly located in the large mesopores (primary channels). Selected area electron diffraction (SAED) patterns of Au/ODMS-C_{16}-550 show spotty diffraction rings which can be exactly assigned to *fcc*-structured Au nanoparticles (Figure 3b, inset). Wide-angle XRD measurements display typical broadened diffraction peaks assigned to *fcc*-structured Au nanoparticles (Figure S6). The mean crystalline size calculated from the Debye–Scherrer formula is about 3.4 nm, slightly larger than the size of small mesopores (the secondary pores) of ODMS-C_{16}-550. Therefore, the Au nanoparticles are actually well confined in the large mesopores, and meanwhile they can be readily accessible for guest molecules through the wormlike secondary small mesopore channels. This kind of nanostructure with a continuum of well-configured hierarchical pores and stably confined Au nanoparticles may have excellent performance in many areas. For comparison, using the same method, Au nanoparticles were loaded into the ordered mesoporous silica templated from EO_{125}-MMA_{174} copolymers, and the obtained sample was denoted as Au/OMS. The reduction of 4-nitrophenol in the presence of $NaBH_4$ was conducted. The results indicate

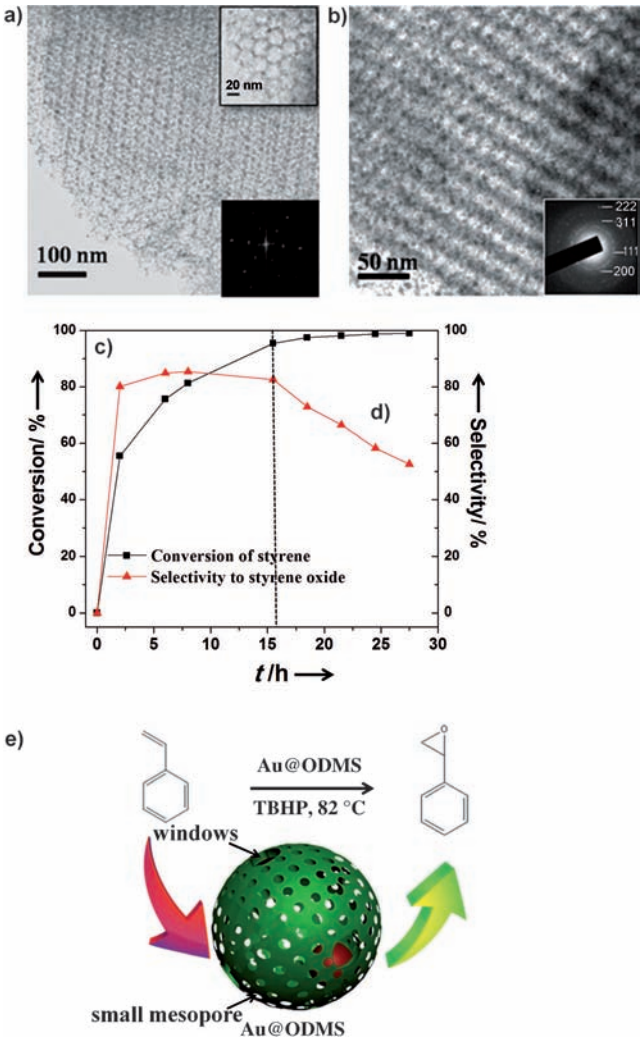

Figure 3. TEM images of Au/ODMS-C_{16}-550, viewed along the a) [110] and b) [211] directions, respectively. Insets in (a) are the corresponding FFT (bottom) and HRTEM images (top). Inset in (b) is the SAED pattern confirming Au nanoparticles of *fcc* structure. c) The conversion of styrene and d) selectivity of styrene oxide at different reaction times. e) Schematic illustration of Au/ODMS-C_{16}-550 with a unique dual-mesopore structure containing Au nanoparticles for high-performance catalysis.

that Au/ODMS-C_{16}-550 has higher reaction rate than Au/OMS under the same conditions, as a result of its unique ordered dual-mesoporous structure (Figure S7).

The obtained Au/ODMS-C_{16}-550 was utilized as a catalyst for the oxidation of styrene using *tert*-butylhydroperoxide (TBHP) as an oxidant under argon atmosphere (Figure 3e). As shown in Figure 3c, the conversion of styrene increases rapidly with the extension of reaction time and reaches 99% at 27 h. This result indicates that the sample Au/ODMS-C_{16}-550 has high catalytic activity. The selectivity of epoxidation reaches about 82% after a reaction time of 15 h and then decreases slightly as the time is prolonged (Figure 3d) owing to the isomerization of styrene oxide or over-oxidation. In a comprehensive evaluation of both conversion and selectivity, Au/ODMS-C_{16}-550 sample displayed high conversion (95.4%) and selectivity (82.6%) after reaction for 15.5 h;

these results are better than most of the heterogeneous catalytic systems reported earlier.[17,4d] The excellent catalytic performance of the dual-mesoporous silica loaded with Au nanoparticles may stem from its unique pore mesostructure and highly dispersed, well-confined uniform small Au nanoparticles.

In summary, a solvent-evaporation-induced step-by-step aggregating assembly process has been developed for the synthesis of ordered dual-mesoporous silica materials in an acidic THF/H_2O solution by using the non-ionic block copolymer PEO-*b*-PMMA and the cationic surfactant C_nTAB as the co-templates. The obtained ordered dual-mesoporous materials show high surface areas (510–670 $m^2 g^{-1}$) and two uniform sets of mesopores with diameters of about 2.5 and 20 nm, with the small mesopores being distributed around the large mesopore. The size of the small mesopore can be readily adjusted independently by using C_nTAB molecules having hydrophobic chains of different lengths. In addition, small Au nanoparticles (about 4 nm in diameter) can be encapsulated in the ordered dual-mesoporous silica. The obtained Au/ODMS materials exhibited excellent performance in catalyzing the epoxidation of styrene with high conversion (95.4%) and selectivity (82.6%) toward styrene oxide. Additionally, it is expected that this co-assembly route using two "soft" templates could be extended to synthesize dual-mesoporous materials with diverse framework compositions like metal oxides, carbon, and organosilica, and it also can serve as a useful strategy for tailoring the pore architecture and size of mesoporous materials for specific separation and catalytic applications.

Experimental Section

EO_{125}-MMA_{174} (PDI: 1.09) was synthesized by the atom radical transfer polymerization (ATRP) method according to our previous report.[18] For the typical synthesis of ordered dual-mesoporous silica, a THF solution of EO_{125}-MMA_{174} (0.67 wt%; 9.0 g) was mixed with C_{16}TAB (60 mg) and 2 M HCl solution (3.0 g), and the mixture was stirred for 2 h before TEOS (0.45 g) was added. The mass ratio of the reactants in this synthesis was set as EO_{125}-MMA_{174}/THF/2 M HCl/TEOS/C_{16}TAB = 1:150:50:7.5:1. After further stirring for 0.5 h, the resulting solution was left to stand in a hood for slow evaporation of THF at 25 °C in air over 48 h. The white precipitate was collected by centrifugation, washed three times with ultrapure water, and dried at 25 °C. The as-made samples were subjected to calcination at 550 °C in air for 5 h to remove the organic template. Detailed information on the loading of Au nanoparticles and catalytic reaction are available in the Supporting Information.

Received: March 21, 2012
Published online: May 13, 2012

Keywords: block copolymers · heterogeneous catalysis · mesoporous materials · self-assembly

[1] a) C. T. Kresge, M. E. Leonowicz, W. J. Roth, J. C. Vartuli, J. S. Beck, *Nature* **1992**, *359*, 710; b) D. Y. Zhao, J. L. Feng, Q. S. Huo, N. Melosh, G. H. Fredrickson, B. F. Chmelka, G. D. Stucky, *Science* **1998**, *279*, 548.

[2] a) M. Hartmann, *Chem. Mater.* **2005**, *17*, 4577; b) J. Fan, C. Z. Yu, T. Gao, J. Lei, B. Z. Tian, L. M. Wang, Q. Luo, B. Tu, W. Z. Zhou, D. Y. Zhao, *Angew. Chem.* **2003**, *115*, 3254; *Angew. Chem. Int. Ed.* **2003**, *42*, 3146; c) Y. H. Deng, D. W. Qi, C. H. Deng, X. M. Zhang, D. Y. Zhao, *J. Am. Chem. Soc.* **2008**, *130*, 28.

[3] a) M. Grün, A. A. Kurganov, S. Schacht, F. Schüth, K. K. Unger, *J. Chromatogr. A* **1996**, *740*, 1; b) J. W. Zhao, F. Gao, Y. L. Fu, W. Jin, P. Y. Yang, D. Y. Zhao, *Chem. Commun.* **2002**, 752.

[4] a) A. Corma, *Chem. Rev.* **1997**, *97*, 2373; b) A. Taguchi, F. Schüth, *Microporous Mesoporous Mater.* **2005**, *77*, 1; c) Y. Wan, D. Y. Zhao, *Chem. Rev.* **2007**, *107*, 2821; d) Y. H. Deng, Y. Cai, Z. K. Sun, J. Liu, C. Liu, J. Wei, W. Li, C. Liu, Y. Wang, D. Y. Zhao, *J. Am. Chem. Soc.* **2010**, *132*, 8466.

[5] C. Y. Lai, B. G. Trewyn, D. M. Jeftinija, K. Jeftinija, S. Xu, S. Jeftinija, V. S.-Y. Lin, *J. Am. Chem. Soc.* **2003**, *125*, 4451.

[6] M. Mamak, N. Coomb, G. Ozin, *J. Am. Chem. Soc.* **2000**, *122*, 8932.

[7] a) P. Yang, T. Deng, D. Zhao, P. Feng, D. Pine, B. F. Chmelka, G. M. Whitesides, G. D. Stucky, *Science* **1998**, *279*, 548; b) T. Sen, G. J. T. Tiddy, J. L. Casci, M. W. Anderson, *Angew. Chem.* **2003**, *115*, 4797; *Angew. Chem. Int. Ed.* **2003**, *42*, 4649; c) Y. H. Deng, C. Liu, T. Yu, F. Liu, F. Q. Zhang, Y. Wan, L. J. Zhang, C. C. Wang, B. Tu, P. A. Webley, H. T. Wang, D. Y. Zhao, *Chem. Mater.* **2007**, *19*, 3271; d) Z. K. Sun, Y. H. Deng, J. Wei, D. Gu, B. Tu, D. Y. Zhao, *Chem. Mater.* **2011**, *23*, 2176.

[8] a) K. Na, C. Jo, J. Kim, K. Cho, J. Jung, Y. Seo, R. J. Messinger, B. F. Chmelka, R. Ryoo, *Science* **2011**, *333*, 6040; b) J. X. Jiang, J. H. Yu, A. Corma, *Angew. Chem.* **2010**, *122*, 3186; *Angew. Chem. Int. Ed.* **2010**, *49*, 3120.

[9] a) B. T. Holland, L. Abrams, A. Stein, *J. Am. Chem. Soc.* **1999**, *121*, 4308; b) L. M. Huang, Z. B. Wang, J. Y. Sun, L. Miao, Q. Z. Li, Y. S. Yan, D. Y. Zhao, *J. Am. Chem. Soc.* **2000**, *122*, 3530; c) A. G. Dong, Y. J. Wang, Y. Tang, Y. H. Zhang, N. Ren, Z. Gao, *Adv. Mater.* **2002**, *14*, 1506.

[10] a) J. H. Sun, Z. P. Shan, T. Maschmeyer, J. A. Moulijn, M. O. Coppens, *Chem. Commun.* **2001**, 2670; b) S. Areva, C. Boissière, D. Grosso, T. Asakawa, C. Sanchez, M. Lindén, *Chem. Commun.* **2004**, 1630; c) K. Suzuki, K. Ikari, H. Imai, *J. Am. Chem. Soc.* **2004**, *126*, 462; d) T. Brezesinski, C. Erpen, K. Iimura, B. Smarsly, *Chem. Mater.* **2005**, *17*, 1683; e) O. Sel, D. Kuang, M. Thommes, B. Smarsly, *Langmuir* **2006**, *22*, 2311; f) Y. H. Deng, J. Liu, C. Liu, D. Gu, Z. K. Sun, J. Wei, J. Y. Zhang, L. J. Zhang, B. Tu, D. Y. Zhao, *Chem. Mater.* **2008**, *20*, 7281.

[11] a) M. Groenewolt, M. Antonietti, S. Polarz, *Langmuir* **2004**, *20*, 7811; b) J. Y. Zhang, Y. H. Deng, J. Wei, Z. K. Sun, D. Gu, H. Bongard, C. Liu, H. H. Wu, B. Tu, F. Schueth, D. Y. Zhao, *Chem. Mater.* **2009**, *21*, 3996.

[12] a) D. C. Niu, Z. Ma, Y. S. Li, J. L. Shi, *J. Am. Chem. Soc.* **2010**, *132*, 15144; b) V. K. Rana, S. S. Park, S. Parambadath, M. J. Kim, S. H. Kim, S. Mishra, R. P. Singh, C. S. Ha, *Med. Chem. Commun.* **2011**, *2*, 1162.

[13] M. Kuemmel, J. H. Smatt, C. Boissière, L. Nicole, C. Sanchez, M. Lindén, D. Grosso, *J. Mater. Chem.* **2009**, *19*, 3638.

[14] a) D. Kuang, T. Brezesinski, B. Smarsly, *J. Am. Chem. Soc.* **2004**, *126*, 10534; b) B. Smarsly, M. Antonietti, *Eur. J. Inorg. Chem.* **2006**, 1111.

[15] J. Wei, H. Wang, Y. H. Deng, Z. K. Sun, L. Shi, B. Tu, M. Luqman, D. Y. Zhao, *J. Am. Chem. Soc.* **2011**, *133*, 20369.

[16] H. G. Zhu, C. D. Liang, W. F. Yan, S. H. Overbury, S. Dai, *J. Phys. Chem. B* **2006**, *110*, 10842.

[17] S. B. Kumar, S. P. Mirajkar, G. C. G. Pais, P. Kumar, R. Kumar, *J. Catal.* **1995**, *156*, 163.

[18] J. Wei, Y. H. Deng, J. Y. Zhang, Z. K. Sun, B. Tu, D. Y. Zhao, *Solid State Sci.* **2011**, *13*, 784.

